PERGAMON

International Journal of Solids and Structures 40 (2003) 6245–6266

INTERNATIONAL JOURNAL OF SOLIDS and STRUCTURES

www.elsevier.com/locate/ijsolstr

Experimental and numerical study of the response of flexible laminates to impact loading

V.B.C. Tan *, V.P.W. Shim, T.E. Tay

Department of Mechanical Engineering, National University of Singapore, 9 Engineering Drive 1, Singapore S117576, Singapore

Received 25 June 2003; received in revised form 25 June 2003

Abstract

Fabrics and flexible laminates comprising highly oriented polymers possess high impact resistance and are often used in flexible armour applications. This study presents an idealized computational model for flexible [0°/90°] polyethylene fiber-reinforced laminates and show how the model can simulate actual impact tests conducted on the laminates. As these materials are viscoelastic, accurate modeling of their impact and perforation responses requires the formulation of constitutive equations representing such behavior. The material is idealized as networks of one-dimensional pin-jointed fiber elements defined by viscoelastic constitutive relations. Three-element viscoelastic Zener models are used as they are simple yet sufficient to account for the effects of intermolecular and intramolecular bonds, as well as viscous slippage between molecular chains, on the mechanical properties of oriented polymeric fibers. The effects of delamination in laminates are also taken into consideration by modeling flexible laminates as two fiber network layers bonded to each other at corresponding element cross-over points in the adjacent layers. Inter-ply bonding is represented by infinitesimal rigid links which break when the inter-ply bond strength is exceeded resulting in delamination between the plies. Predictions of residual velocity, development of deformation and delamination correlate well with experimental results.

Keywords: Flexible laminate; Flexible armor; Ballistics

1. Introduction

The impetus for research on the impact response of fabric composites has come largely from the search for more effective body amour. Advancement in amour technology comprises not so much the development of stronger amour as an adaptation to changes in the threats that new weapons pose. Fabrics and flexible laminates comprising highly oriented polymers possess high impact resistance and are often used in flexible armor applications. Despite numerous attempts at developing light and flexible protection, it was only after nylon fibers became available in the 1930s that a truly anti-ballistic fabric was possible (Laible, 1980a,b). The first modern day flexible armor was made from fabrics of woven nylon yarns.

* Corresponding author. Tel.: +65-6874-8088; fax: +65-6779-1459.
E-mail address: mpetanbc@nus.edu.sg (V.B.C. Tan).

0020-7683/$ - see front matter © 2003 Elsevier Ltd. All rights reserved.
doi:10.1016/S0020-7683(03)00413-X

Ongoing research on fibers has already resulted in new materials of exceptional strength and stiffness. A significant improvement in the ballistic resistance of flexible armor resulted from using stronger materials while largely maintaining similar fabric weave architecture. After nylon in the 1930s, came aramid fibers in the 1970s (Hattery and Hillman, 1991) and ultra high molecular weight polyethylene (PE) in the 1980s. Nylon yarns in ballistic fabrics have now been replaced by such fibers. In the application of flexible armor, fabrics woven from the yarns of these fibers are currently the most common. The introduction of flexible laminated composites reinforced with filaments of these new high tenacity materials marks another revolution in flexible armor. It is claimed that flexible laminates have better ballistic resistance than woven fabrics because weaving introduces crimp or undulations of the yarns. Crimped yarns need to straighten out before they become effective in resisting projectiles, resulting in excessive deflection which in turn increases the probability of blunt trauma.

While reports on the performance of woven fabric armor are now widely available, research into the ballistic resistance of flexible fiber reinforced laminates is still lacking. Most notable reports on flexible laminate armor are from Prevorsek et al. (1991), Prevorsek and Chin (1992) who evaluated the performance of such laminates through extensive impact tests. To date, there is still no widely accepted theory for the perforation of flexible laminate amour. Comprehensive theoretical analysis of terminal ballistics is almost impossible by virtue of the inherent dynamics. Theoretical analysis is presently hampered by a lack of knowledge of the dynamic properties of fibers and their complex internal interactions arising from the inhomogeneity of the material. Most information on ballistic fabrics is from experimental analyses.

Although useful information on residual velocities and ballistic limits can be obtained from impact tests, they do not provide details on the process of ballistic impact and perforation. High-speed photography requires good experimental techniques and is extremely useful in understanding the physical material deformation of the armor. Ballistic penetration processes are increasingly being analyzed using numerical methods and substantiated by experimental verification.

Without easily available closed-form solutions, numerical analysis remains the most feasible way to analyze ballistic impacts on flexible materials. A numerical model for ballistic impact on flexible laminates incorporating the viscoelastic behavior of their constituent yarns is proposed in the present investigation. Ballistic tests are also performed on the laminates to verify the numerical results. Both test and simulation results are analyzed together to provide a better understanding of the mechanisms involved in projectile impact and perforation of flexible laminates.

The present method for simulating the impact perforation of flexible laminates of [0°/90°] extended chain polyethylene (ECPE) fibers stems from an earlier numerical model for woven fabric amour (Shim et al., 1994, 1995; Tan et al., 2001). The flexible laminate is modeled as a network of pin-jointed one-dimensional elements. The model facilitates concurrence with many physical properties and thus has many advantages. Like the model, actual fabrics are orthotropic and have practically zero shear and bending stiffness. Moreover, the elements and nodes are physically equivalent to the yarns and cross-over points. Basically, the laminate is modeled right down to individual yarns. Besides physical correctness, the model reaps the advantages of simplicity and short computational times. Most important of all, it is easy to incorporate viscoelastic properties, yarn breakage and delamination into the model.

2. Spectra Shield laminates

Though flexible laminates are still less common than woven fabric in armor applications, they are gaining acceptance. In 1989, Allied Signal Incorporated commercialized flexible panels of polyethylene fibers called Spectra® which are twenty to thirty times as stiff and three times as strong as nylon. Results of impact tests and computational simulations reported in this paper focuses on Spectra Shield®, a UHMW PE fiber-reinforced laminate. Spectra Shield® comprises two layers of continuous unidirectional Spectra®

Table 1
Properties of Spectra® 1000 fibres, Kraton and Spectra Shield®

Fibre properties	
Tensile modulus	11.9 N/dex
Tenacity	0.209 N/dtex
Elongation at break	2.7%
Specific density	0.97 g/cm^3
Resin properties	
Tensile modulus	21.4 MPa
Elongation at break	1300%
Laminate properties	
Areal density	0.146 kg/m^2
Fibre content	70–80% by weight

PE filaments in a thermoplastic resin, Kraton D1107 (Shell Chemical Company). The resin has a tensile modulus of 21.4 MPa and an elongation to breakage of 1300% (Ash and Ash, 1992). The filaments in the two layers are orthogonal to each other, i.e. the material is a [0°/90°] laminate. The properties of the fibers, resin and laminate are shown in Table 1. The unit of "N/dtex" is common in describing the mechanical properties of fibers and yarns. For a specific density of 0.97 g/cm^3, 1 N/dtex is equivalent to 9.7 GPa. The fiber content is obtained from the reports of Prevorsek et al. (1991) and Lin et al. (1990). It should also be noted that the properties shown represent the mechanical response displayed by the material under quasi-static loading conditions. The dynamic mechanical properties of the material are significantly different and are discussed in later sections. PE fibers are strong because their molecules are highly aligned and their simple molecular structure without side groups ($[CH_2CH_2]_n$) allows dense packing of molecules. With a specific density of 0.97 compared to 1.44 for aramids, PE fibers have even higher specific strengths and tensile moduli than aramids. The main disadvantage of PE fibers is that their strength is reduced at high temperatures and they tend to creep considerably under high tension.

3. Computational simulation and modeling

The progress of research on flexible armor has largely been driven by experimental testing. It is difficult to perform analytical studies on such materials. Although flexible, such materials are different from isotropic membranes because their constituent yarns and fibers impart direction dependent mechanical properties. Advanced flexible armor systems comprise polymeric fibers which exhibit mechanical behavior that is sensitive to strain rate. Hence, the difficulties associated with the analysis of materials under dynamic loads are further compounded by material inhomogeneity and strain-rate dependency. Such complexities make numerical analysis the most viable alternative to predicting the impact response of flexible armor.

3.1. Laminate model

The model proposed in this paper is developed specifically for Spectra Shield® laminates. However, the generality of the formulation makes the model amenable for the simulation of ballistic impact of thin flexible fiber-reinforced laminates, regardless of fiber material direction, fiber material and resin type.

The proposed model is a further development of an earlier numerical model for Twaron®, a cross-woven fabric comprising high strength aramid fibers (Shim et al., 1994, 1995; Tan et al., 2001). In the cross-woven fabric model, the simulation is carried out for a single ply of the material. The material is modeled as a

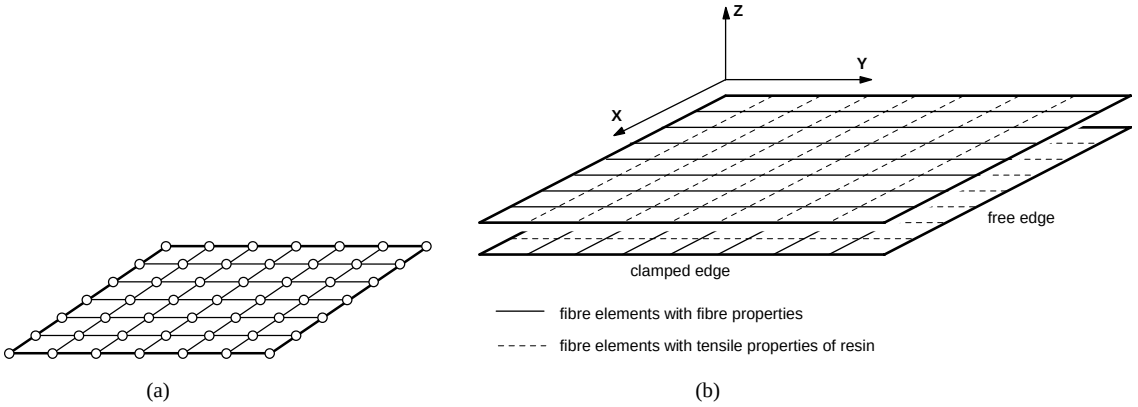

Fig. 1. Numerical model of (a) cross-woven fabric and (b) [0°/90°] flexible laminate.

network of nodes connected together by pin-jointed one-dimensional elements as shown in Fig. 1(a). Each node represents a weave cross-over point and is assigned a mass such that the areal density of the fabric is maintained macroscopically. The interconnecting elements represent the yarns of the fabric and their mechanical response is described by constitutive equations reflecting the behavior of the yarns.

A pin-jointed network inherently implies that the material is totally drapable (i.e. zero bending stiffness) and has no shear stiffness. This is not strictly true for laminates because the resin matrix imparts some degree of bending and shear stiffness. Nevertheless, the present analysis is limited to flexible laminates with only two plies and a non-rigid resin matrix; hence, bending and shear stiffness are negligible. Cross-woven fabrics and Spectra Shield® differ in many aspects because one is a fabric and the other a laminate. Orthogonal yarns in woven fabrics are held together by the weave at cross-over points while filaments in laminates are held together by resin. Delamination is a phenomenon unique to laminates. It is a means of energy dissipation and has been reported to enhance the ballistic resistance of laminates (Kang and Kim, 2000; Morii et al., 1995). In order to model ballistic impact on laminates satisfactorily, delamination must be catered for. A schematic of the laminate model is shown in Fig. 1(b).

3.2. Algorithm

In the present model for [0°/90°] Spectra Shield® laminates, the two laminae of each laminate are modeled as two separate networks. Since each lamina in Spectra Shield® consists of resin impregnated unidirectional filaments, the properties of the elements in each mesh layer are different in different directions. Elements in the direction of the fibers are assigned properties which reflect the mechanical behavior of the fibers while elements in the orthogonal direction are assigned properties which represent the tensile properties of the resin (Fig. 1(b)). The plies are bonded together at cross-over points; i.e. between corresponding nodes of the two networks. Each node is assigned a mass, m, such that the areal density of the laminate is satisfied.

In the computational simulation, the projectile is modeled as a rigid frictionless sphere. The simulation begins with the projectile traveling at the impact velocity at the instant of contact with the laminate. Computation proceeds via small time increments until the laminate starts to tear or the projectile is defeated. The resultant force on each node arising from tension in fiber elements connected to it is first calculated. This resultant determines the acceleration and hence, the change in velocity and displacement of a node. The displacement of the projectile and the nodes of the laminate model are determined from the central time difference integration scheme given by

$$\mathbf{u}_{t+\Delta t} = \mathbf{u}_t + \dot{\mathbf{u}}_{t+\Delta t/2}\Delta t \tag{1}$$

$$\dot{\mathbf{u}}_{t+\Delta t/2} = \dot{\mathbf{u}}_{t-\Delta t/2} + \ddot{\mathbf{u}}_t \Delta t \tag{2}$$

and

$$\ddot{\mathbf{u}}_t = \frac{\sum \mathbf{F}_t}{m} \tag{3}$$

Here, $\mathbf{u}$ is the displacement of a node, $\sum \mathbf{F}$ is the sum of the forces acting on the node and m is the mass of the node. The same equations are used in determining the acceleration, velocity and displacement of the rigid projectile.

The forces acting on a node comprises the axial forces from the four elements connected to it within the same ply. These axial forces are determined from the constitutive equations describing the mechanical properties of the elements. After the total forces acting on all the nodes are determined, the nodal acceleration, velocities and displacements are updated using Eqs. (3), (2) and (1) in sequence.

Up to this stage, the computational process is similar to that of the earlier woven fabric model described in Shim et al. (1994, 1995) and Tan et al. (2001). Computation then continues with the 'delamination' and 'surface interpenetration' subroutines, which check the position of each node in the lower ply to determine if it has debonded from or penetrated the upper ply. When the positions of the nodes have been determined, the tensile force in each fiber element is calculated using the appropriate constitutive equation to determine if an element has failed. Failed elements are flagged and excluded from future computation. The process is repeated until the projectile is defeated (i.e. the projectile velocity changes sign) or the laminate begins to tear.

3.3. Projectile-laminate surface interpenetration

A contact algorithm is formulated to prevent interpenetration between the projectile and laminate surfaces and another to prevent interpenetration between the upper and lower plies after they debond.

The projectile is modeled as a rigid frictionless sphere. At each time step, the velocity and position of the projectile and the velocities and positions of the nodes of the laminate are first updated independently from one another. A search is then made for nodes that have interpenetrated the projectile. For each node that has interpenetrated the projectile, it is pushed to the surface of the projectile. Since frictionless conditions are assumed, the node is pushed out along a radial direction from the center of the projectile. The difference between the corrected and initial nodal positions gives the displacement correction. Inserting this displacement correction into Eqs. (1) and (2) gives the velocity correction and acceleration correction that need to be added to the initial nodal velocity and acceleration to give the corrected values. The acceleration correction is due to the contact force from the projectile. This contact force is obtained from Eq. (3) together with the acceleration correction. By summing the contact force on each node, the total reaction force acting on the projectile that causes the projectile to decelerate can be determined. Thus, at every time step the projectile is decelerated until it is no longer in contact with any nodes of the laminate; an indication that the projectile has either perforated the laminate or has been defeated by the laminate and is rebounding from the impact.

3.4. Inter-ply surface interpenetration

Initially, when nodes on the top and bottom plys are bonded to one another, they are coincident and they displace together. When delamination occurs, some nodes become debonded from one another and are thus no longer constrained to move together. However, the constraint that nodes cannot interpenetrate

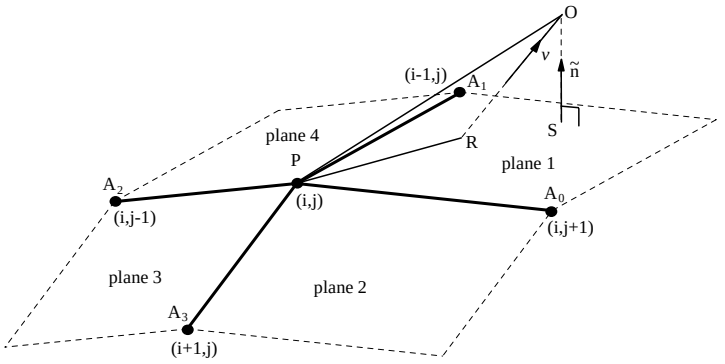

Fig. 2. Surface interpenetration of bottom ply node O into top ply.

adjacent plies must still be enforced. This is accomplished in similar fashion as the algorithm used to correct for the interpenetration of laminate nodes into the projectile.

At each time step, the displacement of all the nodes within a ply is determined independently of nodes within the adjacent ply using Eqs. (1)–(3), i.e. the trajectory of the nodes are determined assuming the absence of an adjacent ply. Nodes from the different plys that are to be bonded to each other are brought together; nodes that are debonded are free to move independently. In some cases, these debonded nodes may interpenetrate the adjacent ply and their positions have to be corrected. An illustration of such a situation is shown in Fig. 2.

In Fig. 2, node O belongs to the bottom ply of the [0°/90°] laminate. It has interpenetrated the top ply after nodal displacements were determined for each ply independently. It is assumed that if a node, O, in the lower ply penetrates the upper ply, the point of penetration in the upper ply is in the vicinity of the node in the upper ply closest to O. In Fig. 2, the node closest to O in the upper ply is P and hence, the point of penetration, R, is assumed to lie on either plane 1, 2, 3 or 4. The algorithm for preventing interpenetration begins with the determination of the point at which node O penetrates the top ply. Nodes in the upper ply are P, A_0, A_1, A_2 and A_3. The velocity of node O is $\boldsymbol{v}$ and $\tilde{\boldsymbol{n}}$ is a unit vector perpendicular to the surface defined by nodes P, A_0 and A_1; SO is the perpendicular distance between O and this surface. Prevention of interpenetration is effected by pushing node P in the direction of $\tilde{\boldsymbol{n}}$ by half the distance SO and by pushing node O by the same amount in the opposite direction.

For each node in the lower ply, the first step of the surface interpenetration subroutine is to determine the node in the upper ply closest to it. To minimize computational time, the node number of the nearest upper node in the previous time step is stored and the search for the nearest node is then confined to that upper node and its four adjacent nodes. This is based on the assumption that, for the explicit code, the time step for stability is also small enough so that there will not be a drastic change in the positions of nodes within one time step. When the nearest upper node is found, the points of intersection of the velocity vector $\boldsymbol{v}$ and each of the four surfaces defined by and containing planes 1, 2, 3, and 4 are determined. Each of these four planes is defined by the node P and two adjacent nodes A_n and A_m (where $n = 0$ and $m = 1$ for the situation depicted in Fig. 2). The vector from P to the point of intersection can be expressed as a sum of the vectors $\boldsymbol{PA_n}$ and $\boldsymbol{PA_m}$. For the surface containing plane 1 shown in Fig. 2, the point of intersection is R and $\boldsymbol{PR}$ can be expressed as

$$\boldsymbol{PR} = \alpha \boldsymbol{PA}_0 + \beta \boldsymbol{PA}_1 \tag{4}$$

where α and β are scalar constants.

Since the point of intersection lies within plane 1 (i.e. between $\boldsymbol{PA}_0$ and $\boldsymbol{PA}_1$), both α and β are positive. For surfaces containing the other planes, the point lies outside the plane and hence, either α or β is negative.

The signs of α and β thus indicate the plane through which the node in the lower ply penetrates the upper ply when interpenetration occurs. Both α or β are positive and less than unity for the plane through which the node interpenetrates. If either α or β is greater than one, it indicates that node P may not be the nearest node and a full search for the nearest node to O needs to be conducted. Once the interpenetrated plane is determined, the perpendicular distance that the lower ply node is above the plane defined by vectors $\boldsymbol{PA}_0$ and $\boldsymbol{PA}_1$ is given by the dot product of $\boldsymbol{PO}$ and $\tilde{\mathbf{n}}$, the upward unit normal to the surface,

$$OS = \boldsymbol{PO} \cdot \tilde{\mathbf{n}} \tag{5}$$

where

$$\tilde{\mathbf{n}} = \frac{\boldsymbol{PA}_0 \times \boldsymbol{PA}_1}{|\boldsymbol{PA}_0 \times \boldsymbol{PA}_1|} \tag{6}$$

If penetration has occurred, then OS is greater than zero. Hence, if a node, O, in the lower ply has penetrated the upper ply between $\boldsymbol{PA}_0$ and $\boldsymbol{PA}_1$, then,

$$\alpha, \beta \quad \text{and } OS > 0 \tag{7}$$

If this condition is met, the displacement of the nearest top node, P, is increased by $1/2\boldsymbol{SO}$, while the displacement of the lower node, O, is reduced by the same amount to exclude interpenetration of the surfaces.

The correction for nodal positions to prevent surface interpenetration is executed only after all nodes in the lower ply have been checked for surface interpenetration. Otherwise, the final position of a node will be affected by adjustments made to neighboring nodes. Hence, instead of making immediate displacement corrections to interpenetrating nodes, their velocities are appropriately adjusted to yield a compatible displacement field at the next time step.

After the displacement correction for a node is determined, its corresponding nodal velocity correction is determined from Eq. (1).

3.5. Delamination

Delamination is an important phenomenon in the impact of laminated structures because the energy expended as a result of delamination has been reported to be significant (Kang and Kim, 2000; Morii et al., 1995). The effectiveness of an armor system in defeating projectiles depends on the amount of projectile kinetic energy it can dissipate during impact. Hence, it is important that delamination be included in the modeling of flexible laminated armor. Besides energy considerations, delamination also affects the integrity of the laminate and consequently the perforation process.

Delamination of the laminate is represented by the debonding of nodes from the top and bottom plys which were initially held together. The criterion for debonding is based on the properties of the resin. A bond strength is specified prior to the computation. As described in the previous section, the nodal positions of each ply are first calculated independently of the adjacent ply. Nodes that were bonded together in the previous time step are brought together if the bond strength is not exceeded. To determine if the bond strength is exceeded, the relative displacement of nodes that were bonded in the previous time step is first determined. The force required to bring two nodes together can then be determined from Eqs. (1)–(3). This means that two nodes initially held together would be debonded if their distance apart exceeds

$$\delta_{\text{debond}} = \frac{\sigma_{\text{D}} \times (L \times \Delta t)^2}{m} \tag{8}$$

Here, σ_{D} is the inter-ply adhesion strength in force per unit area, L is the element length, Δt is the time step and m is the mass of the nodes.

If the force is less than the bond strength, the nodes are brought together. Since all nodes have the same mass, this correction is simply effected by bringing the nodes together at the mean of their initial positions and assigning them the mean of the two velocities. If the force required to bring the nodes together is greater than the bond strength, the nodes are deemed to have debonded and no correction is necessary. The possibility of debonding is only considered when the bottom ply node moves away from instead of interpenetrating the top ply, i.e. when Eq. (5) yields a positive value.

This simple and straightforward method of determining delamination only considers the yield strength of bonds and does not take into account energy release rates for the various modes of delamination. However, it is similar to the delamination model proposed by Cui and Wisnom (1992) which incorporates both stress-based and fracture-mechanics-based approaches to delamination problems. They applied their delamination model to study delamination in three-point bending specimens and tensile specimens with severed central plies and found that the model predicted the onset and growth of delamination accurately. Instead of having only one interface spring link at each node, two springs are used; a spring perpendicular to the surfaces represents the normal strength of the bond and a spring tangential to the surfaces represents the shear strength. Each spring is assumed to be rigid-perfectly plastic with yield strengths equal to the normal and shear yield stresses, respectively and the energy-to-breakage of the springs corresponds to the delamination energy of the laminate. This approach to delamination can be easily accommodated in the present analysis but at present, there is insufficient information on the delamination characteristics of Spectra Shield® to implement such a scheme.

3.6. Constitutive equations

Among other parameters, how well the laminate model represents the actual laminate is greatly dependent on the accuracy of the constitutive equations describing the mechanical properties of the polyethylene Spectra® fibers. For polymers, the influence of viscoelasticity is prevalent. Using static properties to analyze fabric response to ballistic impacts gives rise to misleading results. The lack of knowledge of dynamic material properties is a major hurdle in numerical analyses. Numerous researchers have confirmed the significance of viscoelasticity in impact problems, especially where polymers are concerned. In fiber-reinforced laminates, the main load bearing component of the composite is the fibers. The primary function of the matrix is to bind the filaments together. Spectra Shield® laminates are reinforced by high strength polyethylene fibers. As these materials are viscoelastic, accurate modeling of their impact and perforation responses requires constitutive equations representing such behavior.

Viscoelastic properties are incorporated into numerical analyses via constitutive equations. Dynamic mechanical properties can be represented by a system of Hookean springs and Newtonian dashpots which depict the elastic and viscous components of the modulus. A four-element elastic model (Fig. 3) is often used to idealize polymer behavior because it exhibits the three responses of viscoelastic materials—instantaneous elasticity, delayed elasticity and viscous flow. The accuracy of a constitutive equation depends

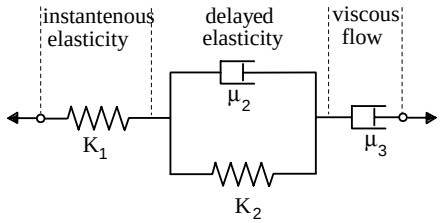

Fig. 3. Four-element viscoelastic model.

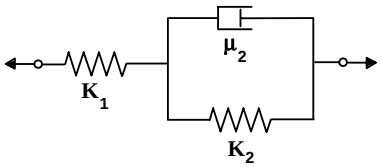

Fig. 4. Three-element viscoelastic (Zener) model.

on the suitability of the selected viscoelastic model. Adding more components to a model improves its accuracy because there are more parameters, but also makes the constitutive equation more complex. Examples of such models being used to replicate the behavior of polymers can be found in the reports by Bland and Lee (1956) and Sogabe and Tsuzuki (1986).

The constitutive equation used in the present model to describe the strain rate sensitivity of Spectra® PE fibers is based on the Zener viscoelastic model shown in Fig. 4. This viscoelastic model is chosen because it is simple, yet can represent the mechanical properties of highly aligned polymeric molecules. In the three-element Zener viscoelastic model, the serial dashpot of the four-element model is omitted because the dashpot accounts for viscous flow which is only pronounced at low frequency loading. For the analysis of ballistic processes, viscous flow can be ignored. The simple Zener material model still possesses both delayed and instantaneous elasticity. It was successfully implemented for simulation PPTA fabrics under impact (Shim et al., 1994, 1995; Tan et al., 2001) where the parameters of the model were assigned values based on the molecular simulation of highly drawn polymeric fibres by Termonia and Smith (1988).

The earliest structural model for PE fibers proposed by Staudinger in the 1930s (Jiang et al., 1992) and models by Peterlin (Narisawa and Yee, 1992) are similar and not much different from the present structural model. Termonia and Smith's (1988) analysis of PPTA fibers is also equally applicable to oriented PE fibers with the use of appropriate values for the strength of the primary and secondary molecular bonds. Since Spectra PE fibers have almost the same molecular structure as PPTA fibers in that the molecules are highly aligned, the three-element model is also adopted for oriented PE fibers. Termonia and Smith's (1988) theoretical model for perfectly oriented PE fibers predicted that tensile strength increases from 1.5 to 7 GPa when the strain rate increases from 0.001667 to 0.1667 s^{-1}; for a strain rate of 1667 s^{-1}, the strength increases further to 24 GPa. A schematic representation of the molecular structure of highly aligned fibers is shown in Fig. 5. Stretching of the fibers causes the molecular chains to extend and also results in the

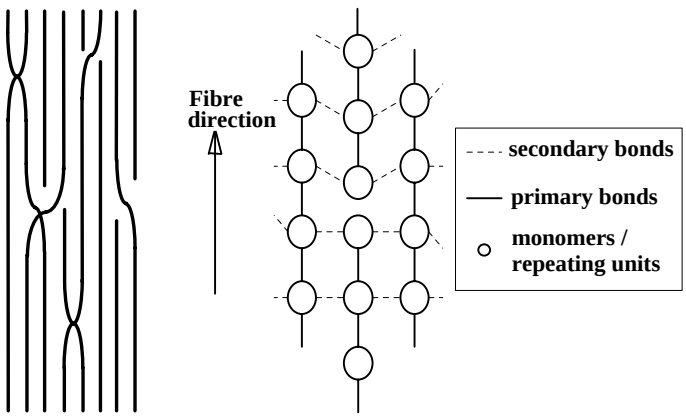

Fig. 5. Termonia and Smith's representation of highly oriented polymeric fibres (Termonia and Smith, 1988).

molecular chains sliding over one another. The extension of the molecular chains is resisted by the strong intramolecular covalent bonds while the sliding of the molecules is resisted by the weaker intermolecular bonds. Essentially, K_1 in the three-element viscoelastic model (Fig. 4) represents the covalent bonds while K_2 represents the collective effect of intermolecular Van der Waals forces acting along the entire molecule. Viscoelasticity results from slippage of molecular chains between each other and is restricted at high deformation rates; this is accounted for in the Zener model by μ_2. The relationship between the stress, σ; strain, ε; and strain rate, $\dot{\varepsilon}$ can be expressed as

$$\left(1+\frac{K_2}{K_1}\right)\sigma+\frac{\mu_2}{K_1}\dot{\sigma}=K_2\varepsilon+\mu_2\dot{\varepsilon} \tag{9}$$

The explicit updating of the stress at each time step is given by

$$\sigma_t=\frac{\mu_2\sigma_{t-\Delta t}+K_1K_2\varepsilon_t\Delta t+K_1\mu_2(\varepsilon_t-\varepsilon_{t-\Delta t})}{(K_1+K_2)\Delta t+\mu_2} \tag{10}$$

Here, Δt is the time step used in the explicit code.

Besides molecular modeling, the strain rate sensitivity of aramid and polyethylene fibers has been investigated experimentally by Prevorsek et al. (1989, 1991). Fibers were hung from a rigid support and impacted by a projectile traveling at 130 m/s. A high-speed camera recording of the impact yields the transverse wave front velocity from which the dynamic modulus, longitudinal wave speed and stress in the fiber can be determined. At the strain rates induced, in the order of 1700 s^{-1}, the calculated dynamic modulus of Spectra® 1000 fibers was 320 GPa, which is almost twice its static value and close to the theoretical limit of 350 GPa. Longitudinal wave speeds were found to be 18,000 m/s. Prevorsek et al. also performed tensile tests on Spectra® 1000 fibers using specimens of very short gauge lengths (75–25 mm) to obtain high strain rates. The tensile modulus as a function of strain rate is plotted in Fig. 6. He found that their tensile modulus increased almost twofold from 12 N/denier (105 GPa) at a strain rate of 0.01667 s^{-1} to 32 N/denier (280 GPa) at 166.7 s^{-1}.

The values of the parameters K_1, K_2 and μ_2 were selected based on Prevorsek's experimental data. It was found that with values of 37.6 N/denier for K_1, 16.8 N/denier for K_2 and 0.565 N s/denier for μ_2 in the three-element model, the tensile modulus as a function of strain rate fitted Prevorsek's experimental data very well, as shown in Fig. 6. The modulus at a particular strain rate is defined by the gradient of the best-fit straight line for the initial part of the stress–strain curve from zero to 1% strain. The stress–strain curves at

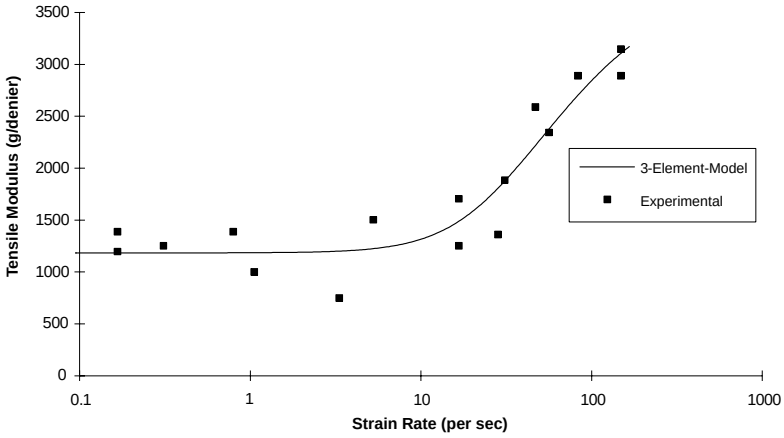

Fig. 6. Tensile modulus of Spectra® 1000 fibres as a function of strain rate (Prevorsek et al., 1991).

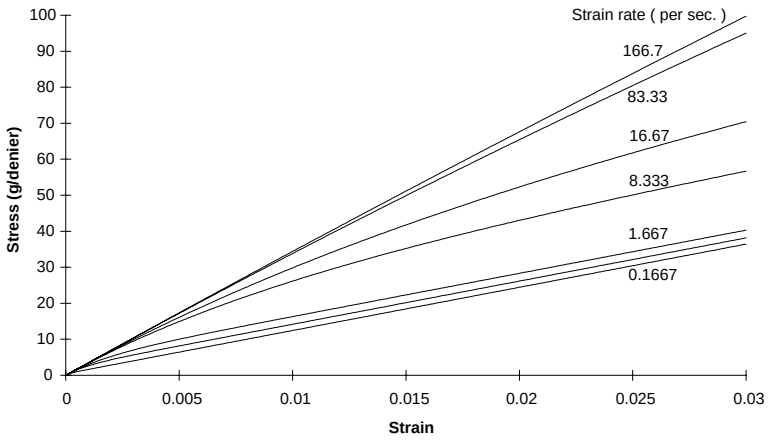

Fig. 7. Stress–strain curves of Zener model.

various strain rates for the three-element model are plotted in Fig. 7. For the three-element viscoelastic model shown in Fig. 4, the limit of the elastic modulus is determined by spring K_1 which occurs when the model is loaded instantaneously. Under extremely high strain rates, intermolecular slippage of the long molecular chains within ECPE fibers is restricted and stretching of the fibers is largely due to the extension of the intramolecular bonds. This is the situation when the stiffness of the fibers approaches the theoretical modulus. The value of 37.6 N/denier is selected for K_1 because it is equivalent to 330 GPa which is approximately the theoretical modulus of ECPE fibers.

Besides their elastic modulus, the strength of PE fibers is also known to be strain rate dependent. At low strain rates, the sliding of molecular chains along one another is dominant and failure occurs when the bonds across molecular chains are broken. At high strain rates, the viscous sliding of molecular chains becomes restricted and hence, the molecular chains are stretched instead and failure occurs when these chains are broken. In order to simulate the ballistic impact on Spectra Shield® to the point of failure, it is also necessary to incorporate the failure of PE fibres into the model. However, Prevorsek et al. (1989, 1991) reported that experimental data on the effects of strain rate on the strength of the fibers were more difficult to obtain than data on tensile modulus because fiber specimens broke at the grips, resulting in great scatter in the data. Based on their experimental results, Prevorsek and Chin (1992) recommend using a tenacity of about 5 GPa and a tensile modulus of 280 GPa for the analysis and design of Spectra® products for absorbing the energy of high-speed projectiles. It has also been reported by Dijkstra and Pennings (1988) and Jiang et al. (1992) that laboratory tests on Spectra® fibers comprising Extended Chain Polyethylene (ECPE) with molecular weights between 5×10^6 and 7×10^6 have recorded tensile strengths of up to 7 GPa and moduli of up to 200 GPa.

While the modulus of high performance PE fibers is close to the theoretical modulus of about 300 GPa for PE crystals, their tensile strength is less than a third of the theoretical value of 30 GPa (Dijkstra and Pennings, 1988). This is explained by Dijkstra and Pennings (1988), who attributed the low strength to the small number of molecular chains connecting the crystalline domains of the microfibrils. Prevorsek et al. (1991) also reported that 75% of ultra drawn PE fibers can be idealized as long crystals connected to small amorphous domains and attributed their excellent impact resistance to the combination of stiff crystals embedded in rubbery amorphous domains. The crystalline domains contain closely packed and perfectly aligned molecular chains. Crystalline domains are connected to one another via a small number of stray molecular chains known as 'tie molecules'. The number of tie molecules is only a fraction of the number of molecular chains in the crystalline domains. Hence, the fibers break at stress levels a fraction of their

theoretical crystalline strength because of the scission of tie molecules. Since the spacing between crystalline domains, l_a, is small compared to the length of the crystalline domains, l_c, the tensile modulus of the fiber, E, is close to modulus of the crystals. The modulus of the fiber is given by

$$E = \frac{\sigma}{\varepsilon} = \frac{\gamma E_c (l_c + l_a)}{\gamma l_c + l_a} \tag{11}$$

where γ is the ratio of the number of tie molecules to the number of molecules in the crystalline domains (Dijkstra and Pennings, 1988).

For $\gamma = 10\%$ and $l_a/l_c = 0.05$, the tenacity of the fiber is 10% of the tenacity of the crystal while its tensile modulus is 70% of the crystal modulus.

In the present analysis, the assumed fiber tensile strength of 7.5 GPa is two and a half times the static strength of 3 GPa and close to the experimental value of 7 GPa reported by Dijkstra and Pennings (1988) and Jiang et al. (1992).

4. Impact tests

Tests were carried out to determine the characteristics of the Spectra® 1000 ECPE flexible laminates under ballistic impact. Data obtained from these tests were used to verify computational results. A high pressure gas gun was used to propel spherical projectiles and thus cause impact perforation of clamped specimens. The projectiles were of 9.5 mm diameter and 3.5 g mass. The test set-up is shown in Fig. 8. Impact velocities ranged from 100 to 400 m/s and both impact and residual velocities were recorded.

Rectangular target specimens were wound around two steel posts and clamped upright 0.5 m from the gun barrel. The target area had dimensions of 110 by 120 mm. Fibers within the ply on the impact side ran in the horizontal direction. A pair of diode lasers and photo diodes (light-sensitive diodes) connected to a counter-timer were used to measure the impact velocity of the projectiles. A different circuit was used to measure the residual velocity of projectiles after they perforated the target. After perforation, the trajectory of the projectiles could be deflected slightly, rendering the laser-diode setup less effective. Each diode was replaced by a screen of parallel thin graphite rods connected in series. The screens were placed in the trajectory of the projectile. As with the laser-diode circuit, breakage of any of the rods by a projectile caused the potential difference across the graphite rod screen to increase, triggering the counter-timer. The graphite rod screen provided a larger projectile detection area compared to single needle-thin laser beams. Graphite

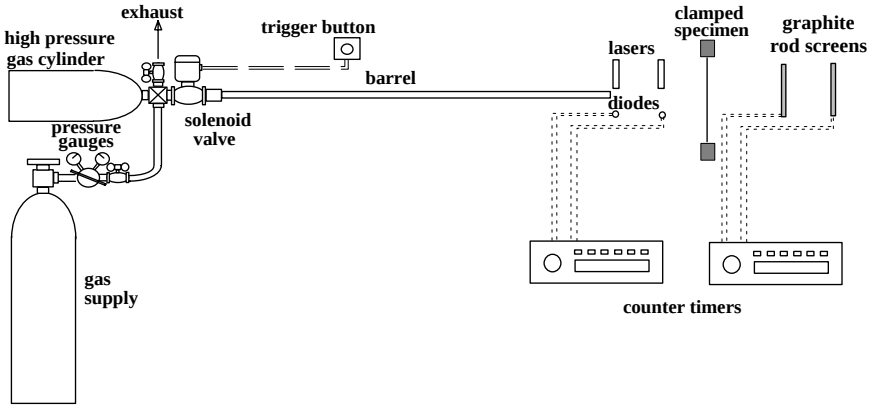

Fig. 8. Schematic diagram of experimental arrangement.

rods are brittle and break easily, so projectile velocity and trajectory were not affected when the projectiles broke the graphite rod screens.

5. Experimental and numerical results

Results from ballistic impact tests on Spectra Shield® are compared with predictions by the proposed numerical model for flexible laminates in terms of residual velocities and energies absorbed by the laminate. Experimental observations such as area of delamination and extent of transverse deflection are also compared to gauge the validity of the numerical analysis. The effects of the filament strength and inter-ply bond strength are studied by varying the parameters in the numerical model. Due to symmetry, only a quarter of the laminate was modeled using 12,000 elements. All elements were 1 mm in length.

5.1. Experimental results

Figs. 9 and 10 show how residual velocity varies with impact velocity and how energy absorbed by the laminate varies with impact energy. The energy absorbed by the laminate is given by the loss in kinetic energy of the projectile. Residual velocity appears to increase linearly with impact velocity. However, an examination of the percentage of impact energy absorbed versus impact energy reveals a steep drop in fraction of impact energy absorbed to 20% as impact energy increases from the ballistic limit to 70 J, after which, the energy absorption declines asymptotically to zero with further increase in impact energy. The relationship between energy absorbed by the laminate and impact energy can be described by

$$\frac{E_{\text{abs}}}{E_{\text{imp}}} = k(E_{\text{imp}})^c \tag{12}$$

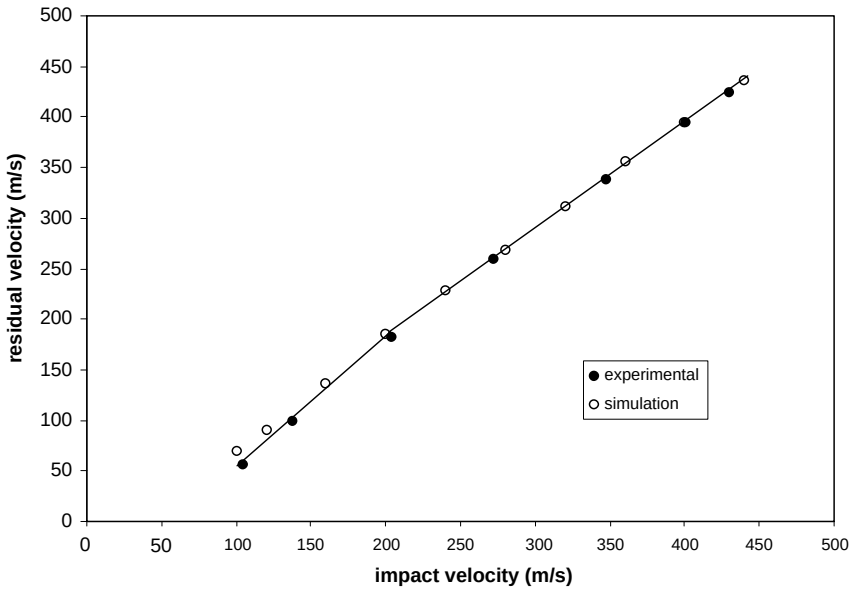

Fig. 9. Relationship between residual and impact velocity.

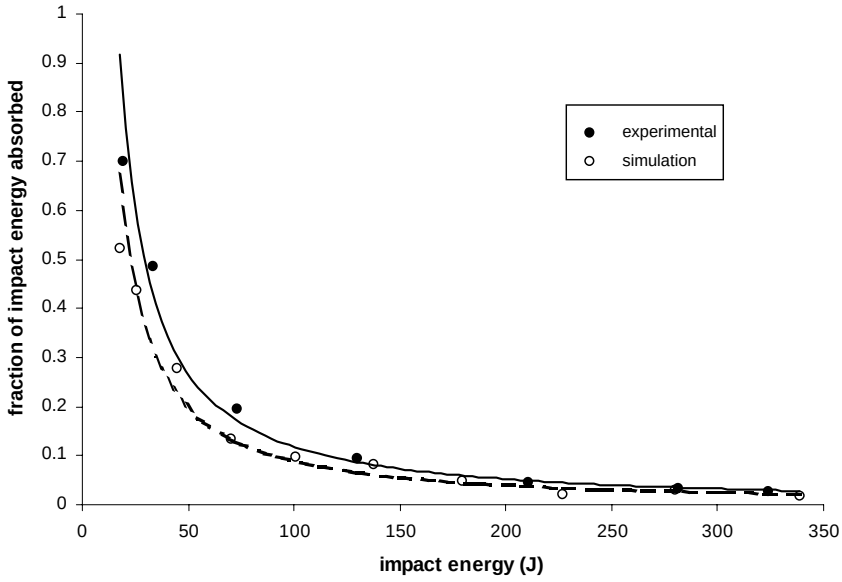

Fig. 10. Variation of fraction of impact energy absorbed with impact energy.

where E_{abs} and E_{imp} denote energy absorbed and impact energy, respectively, and k and c are constants. The best fit equation to the test results is obtained when $k = 26.637$ and $c = -1.177$.

The energy absorption characteristics of Spectra Shield suggest that the material's capacity to dissipate impact energy is strongly dependent on the impact energy. At impact energies just above the ballistic limit of the material, it can still be effective in absorbing a significant fraction of the impact energy. However, this ballistic resistance drops quickly as impact energy increases. Beyond a critical impact energy, the fraction of energy absorbed trails off at a more gradual rate. The range of impact energy from the ballistic limit to the critical impact energy is denoted as low energy (or low velocity) impacts while impacts with energy above the critical impact energy will be termed high energy (or high velocity) impact. The critical impact energy and critical impact velocity are determined to be about 70 J and 200 m/s, respectively. The categorization into low and high velocity impact was made in previous work based on the results involving testing and simulation of woven aramid fabrics (Shim et al., 1994, 1995; Tan et al., 2001).

The energy absorption trend is not the only indicator that there is a discernible transition of the ballistic resistance of the laminate from low to high velocity impacts but associated with the transition are also damage characteristics that can be observed visually in post-impact specimens. Extensive stretch marks were found on specimens when they are perforated just above the ballistic limit but below the critical velocity. Figs. 11 and 12 show specimens perforated below and above the critical impact velocity, respectively.

At low impact velocities, the stretch marks extend from the impact point to the clamped edges. From these marks, it is evident that the entire laminate is deflected and tautly stretched during the impact process. This phenomenon is not found in specimens perforated at very high velocities. For high velocity perforation, stretch marks are absent and damage is localized at the point of impact and perforation. Lines were marked on the specimens before each impact test to indicate where the specimens were clamped. It was observed that at low impact velocities, the lines were pulled slightly inwards away from the clamps. Such displacements of the markings were not observed for high velocity impacts. This is an indication that low velocity impacts tend to stretch the laminate significantly while minimal forces are transmitted to the clamps during high velocity impacts. Similar patterns are found for delamination between the two plys of

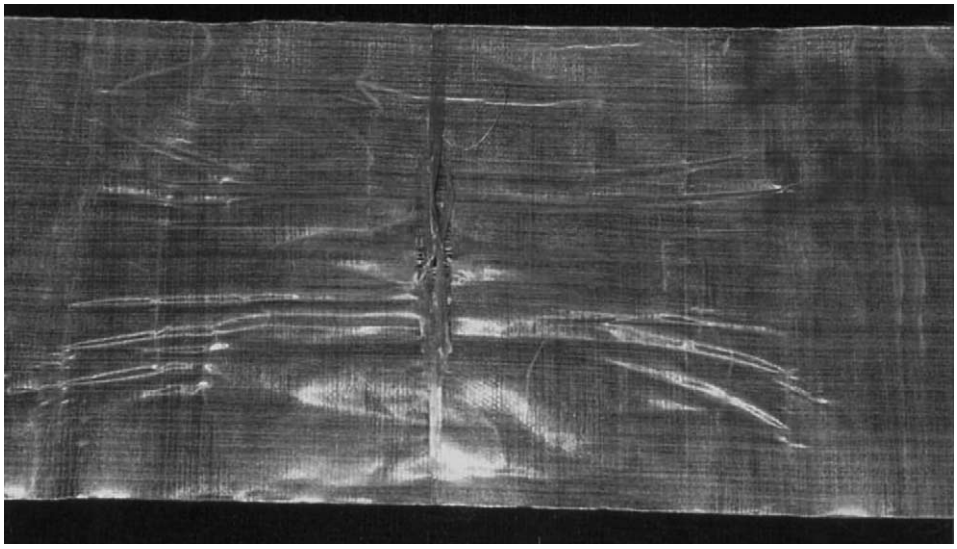

Fig. 11. Material specimen after impact perforation at 104 m/s.

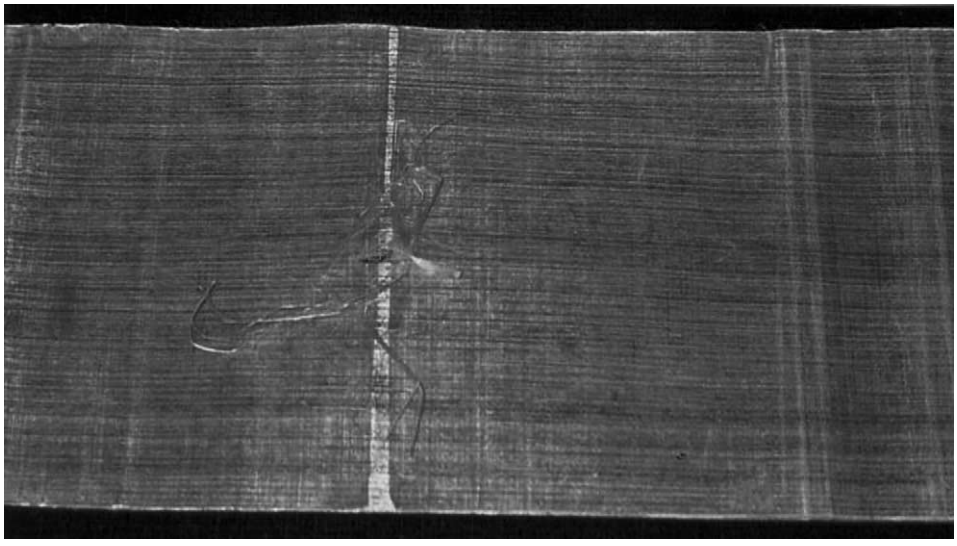

Fig. 12. Material specimen after impact perforation at 401 m/s.

the laminate for low and high energy impacts. During perforation, clamped filaments on the impact face are struck and broken by the projectile, while unclamped filaments in the distal ply debond from the laminate and are pushed away. The area of delamination is invariably diamond-shaped. At high impact velocities, the entire length of some unclamped filaments in the distal ply are delaminated, while at low velocities, the portions near the free edges do not suffer debonding. Perforation holes on the specimens are invariably square because of the orthogonal arrangement of the filaments.

5.2. Comparison between numerical and experimental results

A series of numerical analyses simulating the impact tests were carried out using the proposed model incorporating the constitutive relationships discussed previously. The experimental values of residual velocities are plotted together with the predicted values in Fig. 9. The numerical predictions correlate very well with experimental results. It can be seen that although the relationship between residual velocity and impact velocity is almost linear, a bilinear relationship, with a slightly steeper gradient for impact velocities less than the critical impact velocity of 200 m/s, gives a better correlation. This relationship is also predicted by the numerical simulation. The predicted values of energy absorbed by the laminate model also show good correlation with experimental results, as seen in Fig. 10. As with experimental results, the energy absorption characteristics of the laminate model display a low impact energy regime, where the fraction of energy absorbed drops sharply with impact energy, before the decrease in the energy absorption ratio tapers off towards zero.

Besides good agreement between the experimental and computed residual velocities and energy absorbed by the laminate, the computational model also predicted sequences of the process of impact and laminate deformation that are consistent with the observations from perforated specimens.

Fig. 13 shows the deformation of Spectra Shield® laminates just prior to perforation for an impact velocity of 100 m/s. Due to symmetry, only a quarter of the fabric was modeled in the simulation. The deformation shown is typical of low velocity impacts. At this low impact velocity, the entire laminate is deflected and the projectile starts to penetrate the laminate at about 150 μs after impact. At this instant, the impact point has deflected by about 14 mm. The laminate deformation prior to penetration for high velocity impacts is shown in Fig. 14. In contrast to low velocity impacts, only material in the vicinity of the impact point is deflected. For an impact velocity of 400 m/s, penetration begins at about 12 μs and the deflection of the point of impact is only 4.7 mm. The evidence of extensive fabric deformation for low velocity impacts as predicted by the numerical simulation can be seen in the extensive stretch marks on an actual material specimen impacted at 104 m/s, as shown in Fig. 11. This gives an indication that the entire specimen was deflected. In contrast, a specimen after high velocity impact displayed minimal stretch marks as shown in Fig. 12, supporting simulation results that high impact velocities give rise to localized deformation.

Another feature that is correctly predicted by the numerical model is the pyramidal shape of the deflection. For isotropic membranes, a conical deflection can be expected to propagate outwards from the impact point. Such observations of pyramidal deformation were also recorded by Prevorsek et al. (1991), Prevorsek and Chin (1992) through high-speed photography of ballistic impacts on Spectra Shield® laminates. High-speed photographs showed Spectra Shield® laminates deflecting into the shape of a pyramid centered at the impact point. The transverse deflection proceeded at a much slower rate than the calculated longitudinal stress wave. Four stages in the impact process were observed - localized compression of the target, fiber breakage in several layers, partial penetration with severe delamination and final mushrooming of the projectile as it is arrested. These four stages cannot be observed in both the current impact tests and simulation namely because the current investigation is focused on a single [0°/90°] laminate; however, the current model correctly replicates the pyramidal deflection propagating from the impact point at a much slower rate than the longitudinal stress waves as observed by Prevorsek. The pyramidal deflection is due to the orthogonal directions of the yarns. The transverse deflection wavefront travels faster along the yarns than in other directions, giving rise to the distinctive pyramidal deformation.

Finally, a comparison is made between the extent of delamination predicted by the simulation and observed delamination patterns. Figs. 11 and 12 show that the delaminated areas of the perforated laminates are diamond-shaped and elongated towards the free ends. Using a bond strength equivalent to four times the yield strength of the resin in the numerical simulation gives similar delamination patterns as shown in Figs. 13 and 14. Again, only a quarter of the laminate is shown. The simulation showed that for

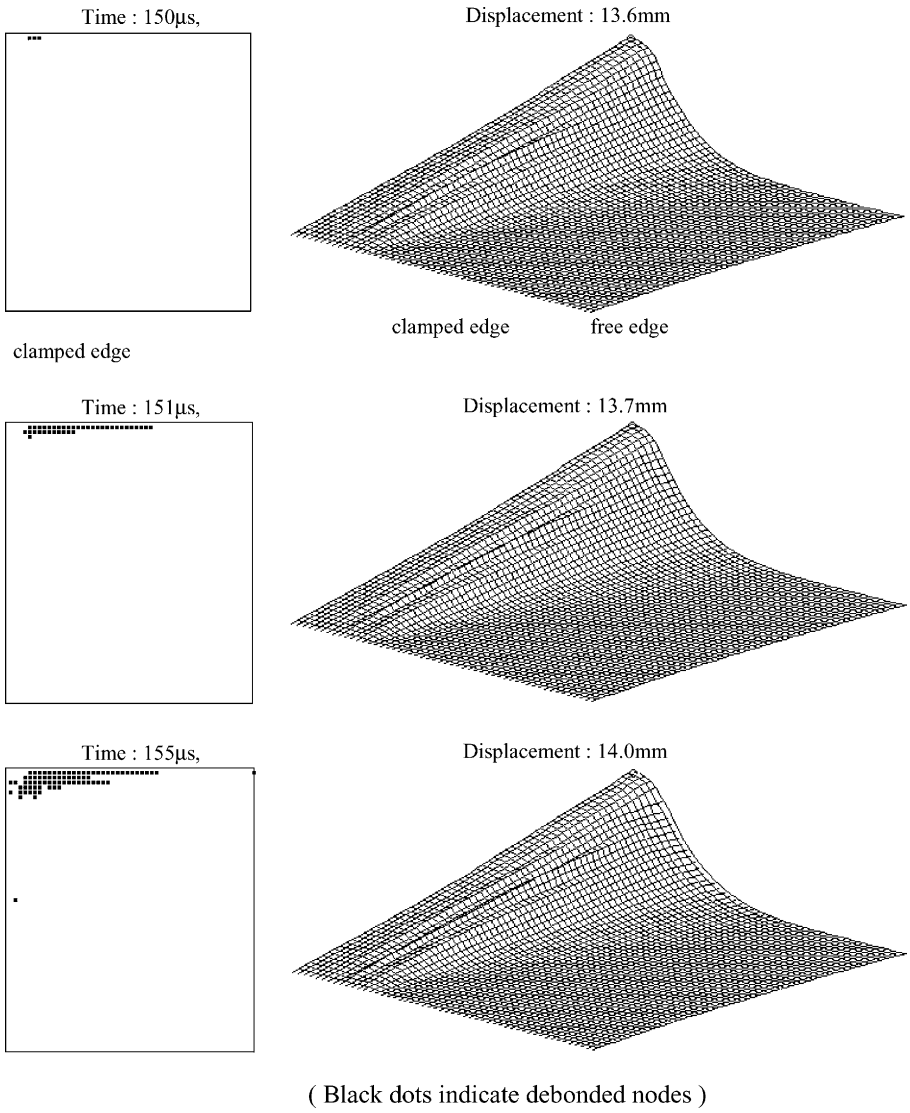

Fig. 13. Development of deformation and delamination at impact of 100 m/s.

low velocity impacts, delamination begins at an advanced stage of the impact process, normally just before penetration occurs. For high velocity impacts, delamination initiates from the impact point almost immediately on impact.

At an impact velocity of 100 m/s, the predicted area of delamination is diamond-shaped and elongated in the direction of the free edges (Fig. 13). At high impact velocities, the predicted delamination is also diamond-shaped but it extends to the free edges and unclamped filaments in the back ply traversing the contact area of the projectile are completely debonded from the laminate (Fig. 14). Fig. 13 also shows that delamination only starts 150 μs after impact when the projectile velocity has dropped from 100 to 70 m/s and when the laminate is just about to tear. When a laminate is struck by a low velocity projectile, filaments traversing the contact area of the projectile in both directions experience high stress levels. Clamped

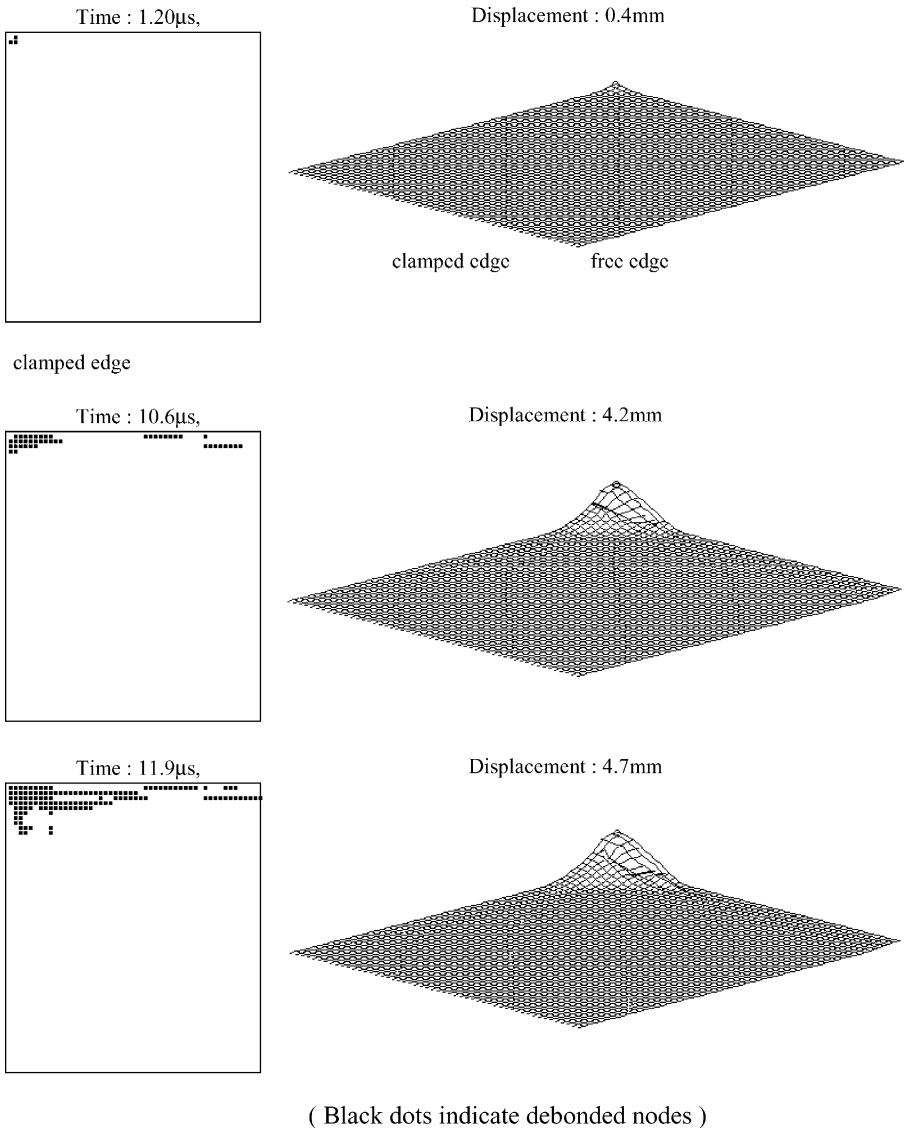

Fig. 14. Development of deformation and delamination at impact of 400 m/s.

filaments are highly stressed because they are restrained at the boundaries. Unclamped filaments at the centre of the laminate are pulled inwards during impact but their motion is resisted by orthogonal filaments bonded to them. Hence, inter-ply bonds on unclamped filaments traversing the area of impact are subjected to high shear stresses. This results in preferential debonding along central unclamped filaments, which leads to an elongated diamond-shaped delamination area.

In contrast to low velocity impacts, laminates subjected to impacts above the critical velocity delaminate upon impact and delamination seems to propagate initially along both clamped and unclamped filaments. This is due to the high inward velocity induced in filaments struck by the projectile. The high velocity generates a shear in inter-ply bonds sufficient to exceed the bond strength, thus causing debonding between

clamped and unclamped filaments. After the tensile stresses have reflected from the boundaries, clamped filaments are restrained by tensile forces rather than shear stresses in inter-ply bonds, thus, delamination begin to propagate preferentially along unclamped filaments.

5.3. Effects filament tenacity and bond strength

As reported by Prevorsek et al. (1989, 1991), the dynamic strength of the PE filaments within Spectra Shield® is not easily determined and hence, a parametric study was carried out to determine the effects of filament tenacity. The bond strength between nodes of the top and bottom plys was another parameter that was studied because of the lack of data on the delamination of Spectra Shield® laminates. Each parameter was increased in two steps—by 25% and 50%—from the initial values of 7.5 GPa for filament strength and 84 MPa for bond strength. Other essential information on the dynamic properties of PE filaments are obtained from Prevorsek's experimental data (1989, 1991).

The maximum energy absorbed by the laminate is predicted to increase from 12 J to 16 J (30% increase) and 18 J (50% increase) when σ_{max} is increased 25% and 50%, respectively. The critical impact energy also increases from 50 J to about 80 J. These increases are due to the higher energy-to-breakage of the fiber elements, which allows the laminate to absorb more energy before it starts to tear. The delamination area, when the laminate begins to tear, is also affected by changes in σ_{max} as shown in Figs. 15 and 16. The fiber elements can withstand higher stress levels and since forces are transmitted to filaments not in contact with the projectile via bonds at cross-over points, the bonds are also subjected to higher stress levels, resulting in more widespread delamination.

When the inter-ply bond strength, σ_D, is increased by 25%, the maximum energy absorbed and critical impact energy increase to about 18 J (50% increase) and 100 J (100% increase) respectively. The effects of increasing the inter-ply bond strength by 50% are similar. This further emphasizes the importance of delamination as a means of energy dissipation and concurs with the work reported by Kang and Kim (2000) and Morii et al. (1995). As expected, the delamination area when the laminate begins to tear is reduced with increased inter-ply bond strength. At an impact velocity of 100 m/s, no delamination was predicted, even when the laminate started to tear. Delamination was predicted only for impact velocities greater than 200 and 280 m/s when σ_D was increased by 25% and 50%, respectively. The reduction in delamination area for an impact velocity of 400 m/s when σ_D is increased by 50% is shown in Fig. 17.

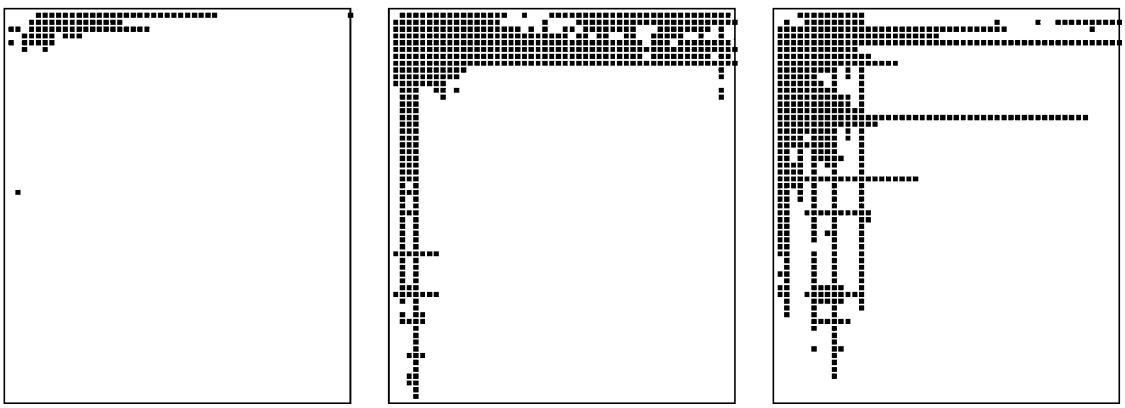

Fig. 15. Effect of fibre strength, σ_{max}, on delamination area (impact velocity = 100 m/s).

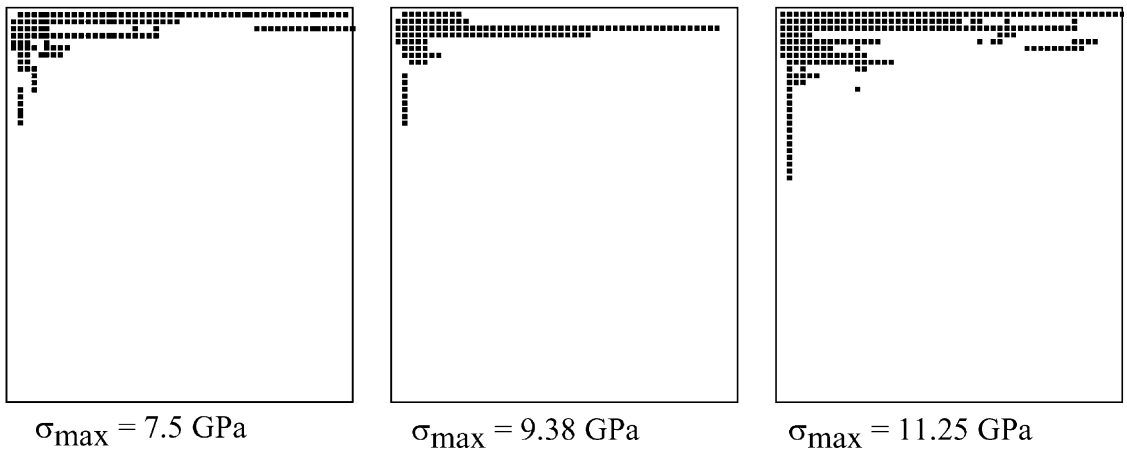

Fig. 16. Effect of fibre strength, σ_{max}, on delamination area (impact velocity = 400 m/s).

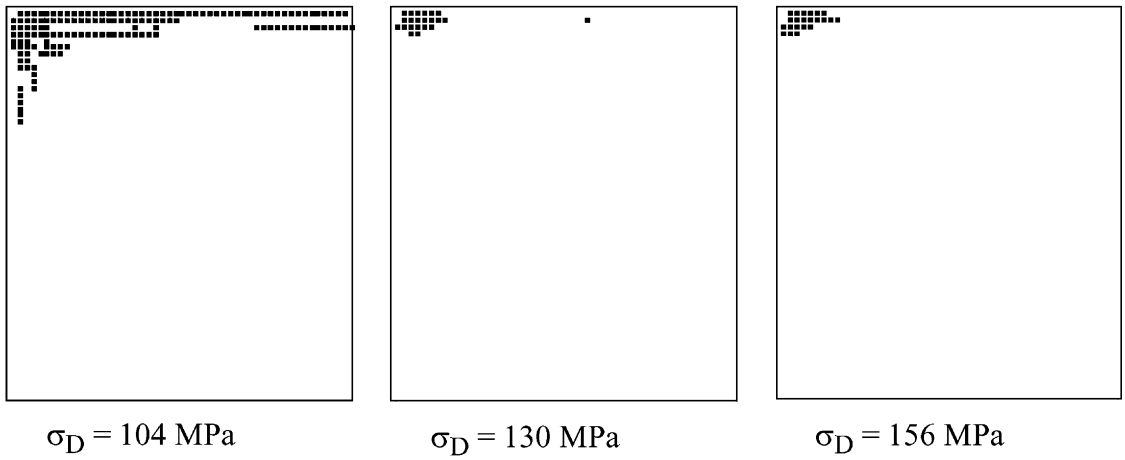

Fig. 17. Effect of inter-lamina bond strength, σ_D, on delamination area (impact velocity = 400 m/s).

6. Conclusions

A physically realistic theoretical model has been proposed for simulating small projectile impact and perforation of [0°/90°] flexible fiber-reinforced laminates. The model is simple to implement and gives an accurate description of the perforation process. The laminate is modeled as two networks of nodes joined together by one-dimensional elements. The two networks are initially bonded to each other and can debond to simulate delamination. Ballistic tests on Spectra Shield® laminates yielded experimental data which verified numerical predictions both quantitatively and qualitatively. The experimental and numerical results correlate closely in terms of projectile residual velocity and energy absorbed. The model is also able to predict the manner in which the flexible laminate deforms and tears at the impact point. The presence of stretch marks and delamination in laminate specimens are accurately replicated by the model. The numerical model correctly predicts local deformation of the laminate at high velocity impacts and extensive deflection at low velocity impacts. The pattern of delamination in post-impact specimens is observed to be

always diamond-shaped. This is also shown in the numerical results, which also show delamination initiating differently for low and high velocity impacts.

A significant factor in the accuracy of the proposed model is the inclusion of viscoelasticity (strain rate sensitivity). Viscoelastic effects are incorporated into the constitutive equations by using a linear three-element viscoelastic model. This idealization is used because it represents the important mechanical responses of instantaneous and delayed elasticity, which are significant in most polymeric materials including Spectra® 1000 fibers. The parameters used in the viscoelastic model for the constitutive equation for Spectra Shield® laminates are determined from published experimental data. In addition to viscoelasticity, the effect of inter-ply bond strength of laminates is also found to affect the accuracy of the theoretical model.

Analysis of Spectra Shield® laminates is hampered by the lack of information on its delamination criteria. Nevertheless, primary observations of dynamic deformation and failure are adequately accounted for despite these shortcomings.

Acknowledgement

This work was partially supported by Honeywell Holdings (Thailand) Co., Ltd., who provided Spectra Shield® laminate samples.

References

Ash, M., Ash, I., 1992. Handbook of Plastic Compounds, Elastomers and Resins. VCH Publishers.

Bland, D.R., Lee, E.H., 1956. On the determination of a viscoelastic model for stress analysis of plastics. J. Appl. Mech. 23 (3), 416–420.

Cui, W., Wisnom, M.R., 1992. A combined stress-based and fracture-mechanics-based model for predicting delamination in composites. Composites 24 (6), 467–474.

Dijkstra, D.J., Pennings, A.J., 1988. The role of taut tie molecules on the mechanical properties of gel-spun UHMWPE fibers. Polym. Bull. 19, 73–80.

Hattery, G.R., Hillman, M.E.D., 1991. High Performance Organic Fibers for Polymeric Composites, High Performance Polymers. Hanser Publishers. pp. 255–278.

Jiang, H., Adams, W.W., Eby, R.K., 1992. High performance polymer fibers. In: Materials Science and Technology. Weinheim Publishers. pp. 597–631.

Kang, T.J., Kim, C., 2000. Energy-absorption mechanisms in Kevlar multiaxial warp-knit fabric composites under impact loading. Compos. Sci. Technol. 60 (5), 773–784.

Laible, R.C., 1980a. History of Armor, Penetration Mechanics of Textile Structures, Ballistic Materials and Penetration Mechanics. Elsevier Scientific Publishing Company. pp. 22–35.

Laible, R.C., 1980b. Fibrous Armor, Penetration Mechanics of Textile Structures, Ballistic Materials and Penetration Mechanics. Elsevier Scientific Publishing Company. pp. 73–113.

Lin, L.C., Bhatnagar, A., Chang, H.W., 1990. Ballistic energy absorption of composites. In: 22nd International SAMPE Technical Conference, pp. 1–13.

Morii, T., Hamada, H., Hiroyuki, D., Desaeger, M., Gotoh, A., Yokoyama, A., Verpoest, I., Maekawa, Z., 1995. Damage tolerance of glass mat/epoxy laminates hybridized with flexible resin under static and impact loading. Compos. Struct. 32 (1-4), 133–139.

Narisawa, I., Yee, A.F., 1992. Crazing and fracture of polymers. In: Materials Science and Technology. Weinheim Publishers. pp. 736–745.

Prevorsek, D.C., Chin, H.B., 1992. Origins of damage tolerance in polythene fibers and composites. In: 24th International SAMPE Technical Conference, pp. T307–T318.

Prevorsek, D.C., Kwon, Y.D., Harpell, G.A., Li, H.L., 1989. Spectra® composite armor: dynamics of absorbing the kinetic energy of ballistic projectiles. In: 34th International SAMPE Symposium, pp. 1780–1789.

Prevorsek, D.C., Chin, H.B., Kwon, Y.D., Field, J.E., 1991. Strain rate effects in ultrastrong polyethylene fibers and composites. J. Appl. Polym. Sci.: Appl. Polym. Symp. 47, 45–66.

Shim, V.P.W., Tan, V.B.C., Tay, T.E., 1994. Modelling deformation and damage characteristics of woven fabric under small projectile damage. Int. J. Impact Eng. 16 (4), 585–605.

Shim, V.P.W., Tan, V.B.C., Tay, T.E., 1995. Perforation of woven fabrics by spherical projectiles. Impact Waves Fract. AMD 205, 293–306.

Sogabe, Y., Tsuzuki, M., 1986. Identification of dynamic properties of linear viscoelastic materials by the wave propagation testing. Bull. Jpn. Soc. Mech. Eng. 29 (254), 2410–2417.

Tan, V.B.C., Shim, V.P.W., Lee, N.K., 2001. Computational analysis of oblique projectile impact on high strength fabric. In: Fourth International Symposium on Impact Engineering, pp. 327–332.

Termonia, Y., Smith, P., 1988. A Theoretical Approach to the Calculation of the Maximum Tensile Strength of Polymer Fibers, High Modulus Polymers. Marcel Dekker Inc.. pp. 321–362.